nature communications

Article

https://doi.org/10.1038/s41467-024-53981-0

The BAF complex enhances transcription through interaction with H3K56ac in the histone globular domain

Received: 15 April 2024

Accepted: 28 October 2024

Published online: 07 November 2024

Check for updates

Kwangbeom Hyun[1], Jihye Ahn[1], Hyoungmin Kim[1], Jihyun Kim[1], Yong-In Kim[2], Hee-Sung Park[3], Robert G. Roeder[4], J. Eugene Lee[5] ✉ & Jaehoon Kim[1] ✉

Histone post-translational modifications play pivotal roles in eukaryotic gene expression. To date, most studies have focused on modifications in unstructured histone N-terminal tail domains and their binding proteins. However, transcriptional regulation by chromatin-effector proteins that directly recognize modifications in histone globular domains has yet to be clearly demonstrated, despite the richness of their multiple modifications. Here, we show that the ATP-dependent chromatin-remodeling BAF complex stimulates p53-dependent transcription through direct interaction with H3K56ac located on the lateral surface of the histone globular domain. Mechanistically, the BAF complex recognizes nucleosomal H3K56ac via the DPF domain in the DPF2 subunit and exhibits enhanced nucleosome-remodeling activity in the presence of H3K56ac. We further demonstrate that a defect in H3K56ac–BAF complex interaction leads to impaired p53-dependent gene expression and DNA damage responses. Our study provides direct evidence that histone globular domain modifications participate in the regulation of gene expression.

Highly conserved histone proteins undergo several types of covalent modifications that can either directly alter the chromatin architecture or create docking sites for specific domains in chromatin-effector proteins, processes that are central to epigenetic regulation[1,2]. Misinterpretation of histone modification marks may serve as a general mechanism for many human diseases[3–5]. An essential step in understanding the mechanistic basis for the participation of histone modifications in controlling cellular processes is identifying and characterizing the histone-modifying enzymes and downstream effector proteins responsible for recognizing specific histone marks and translating them into specific biological outcomes[6]. The main focus of studies in recent decades has been on modifications in the unstructured N-terminal tails of histones, which are readily accessible to effector proteins. Many of these studies have relied on short synthetic histone tail peptides, which do not mimic native physiological nucleosome structure, for identification of modification-binding proteins[7]. Recent advances in mass spectrometry have enabled the identification of numerous modifications at various sites within histone globular domains, which have been implicated in chromatin assembly, remodeling, transcription, and genomic instability[8]. Unlike N-terminal tails, histone globular domains form a highly organized structure through extensive histone-histone interactions and interactions with DNA enwrapping them, creating an environment significantly different from that of tails[9,10]. These differences compel the use of physiologically relevant nucleosomes as bait for screening effector proteins that recognize modifications on histone globular

[1]Department of Biological Sciences, Korea Advanced Institute of Science and Technology, Daejeon 34141, South Korea. [2]Center for Bioanalysis, Korea Research Institute of Standards and Science, Daejeon 34113, South Korea. [3]Department of Chemistry, Korea Advanced Institute of Science and Technology, Daejeon 34141, South Korea. [4]Laboratory of Biochemistry and Molecular Biology, The Rockefeller University, New York, NY 10065, USA. [5]Division of Biomedical Metrology, Korea Research Institute of Standards and Science, Daejeon 34113, South Korea. ✉e-mail: jinhwan.lee@kriss.re.kr; kimjaehoon@kaist.edu

domains; however, successful applications of such approaches have not yet been reported.

Histone H3 lysine 56 acetylation (H3K56ac) is a conserved globular domain modification close to the DNA entry-exit site on the lateral surface of the nucleosome core particle[11]. Early studies implicated H3K56ac marks in several cellular processes, including transcription, by virtue of their influence on the assembly and disassembly of nucleosomes[10]. Because newly synthesized H3 in yeast is marked by H3K56ac[12], preferential enrichment of H3K56ac around transcription start sites of actively transcribing genes[11] may be a consequence of the extensive histone exchange that occurs during transcription. H3K56ac marks have also been proposed to increase nucleosome 'breathing' by loosening the nucleosome's grip on the DNA entry-exit site[13], possibly creating an opportunity for interactions with effector proteins and thus causing active transcription. However, the latter mechanism has not been clearly demonstrated because key players have not been reported to directly bind to nucleosomal H3K56ac.

Mammalian switch/sucrose non-fermentable (mSWI/SNF) is a subfamily of ATP-dependent chromatin-remodeling complexes[14] whose members assemble combinatorially with proteins encoded by 29 genes, including multiple paralogs[15]. Considerable attention has been paid to mSWI/SNF because the genes encoding its subunits show high mutational frequencies across a range of human diseases[16]. Strikingly, more than 20% of human cancers have been found to harbor mutations in mSWI/SNF complex subunit genes[15,17], highlighting critical roles of mSWI/SNF in many cellular processes. The presence of various domains capable of interacting with DNA or histone modifications in complex subunits[16] suggests that mSWI/SNF participates in fine-tuning gene expression; notably, failure of this function causes mis-regulation of genes associated with diseases[18,19]. In the context of our current study, H3K56ac was reported to modestly increase nucleosome remodeling by yeast SWI/SNF[13]; however, direct interaction of the mSWI/SNF complex with nucleosomal H3K56ac has not been clearly demonstrated.

In this study, using H3K56ac as a model, we forward-screened for chromatin-effector proteins that directly bind to post-translational modifications located on the globular domain of histones. We demonstrate that, among mSWI/SNF chromatin-remodeling complex subfamily members, the BRG1/BRM-associated factor (BAF) complex specifically and directly binds to nucleosomal H3K56ac through the double PHD finger (DPF) domain in its DPF2 subunit. We also provide mechanistic insight into BAF complex-mediated transcriptional activation of p53-dependent genes, showing that this process involves enhanced chromatin remodeling achieved by direct H3K56ac–BAF complex interaction. Our study provides direct evidence that covalent modifications on histone globular domains also participate in transcriptional regulation through direct interactions with transcription factors.

Results

H3K56ac directly stimulates transcription in vitro

Histone acetylation generally causes transcriptional activation by altering chromatin structure and/or recruiting epigenetic factors, such as histone-modifying enzymes and chromatin remodelers[20,21]. Because histone acetyltransferases (HATs) (e.g., p300, CBP and PCAF in mammalian cells) deposit acetylation at multiple sites on all four core histones[22], the transcriptional impact of individual acetylation at a lysine residue on histones has not been clearly demonstrated. To address this, we generated a series of histone octamers containing histone H3 (H3) acetylated on single lysine residues (Supplementary Fig. 1a) and assembled them into recombinant chromatins with p53ML plasmid[23] using the ACF/NAP1 (ATP-utilizing chromatin assembly and remodeling factor/nucleosome assembly protein 1) system (Supplementary Fig. 1b). We then tested their direct effect on transcription in a cell-free in vitro transcription assay that employs purified p53 and p300 (Supplementary Fig. 1b) as transcription activator and coactivator, respectively, according to the procedure outlined in Supplementary Fig. 1c. Among six individual acetylations in the H3 N-terminal domain, four acetylation types (H3K4ac, H3K9ac, H3K14ac, and H3K18ac) modestly changed transcription relative to that of unmodified H3 (Fig. 1a). In contrast, two acetylation types – H3K23ac and H3K27ac – located close to the nucleosome core, substantially increased transcription. Interestingly, we also found that H3 modified in its globular by H3K56ac exhibited significantly enhanced (~3.4-fold) p53- and p300-dependent transcription relative to unmodified H3. Recombinant chromatin assembled with an H3K56R octamer (Supplementary Fig. 1d), in which H3K56 cannot be acetylated by p300 in our in vitro transcription system, displayed decreased transcription (~0.7-fold) compared with unmodified-chromatin (Fig. 1b), suggesting that acetylation at H3K56 indeed contributes to enhanced transcription.

Recombinant chromatin assembled with unmodified H3, H3K56ac, or H3K56R showed similar micrococcal nuclease (MNase) digestion patterns (Supplementary Fig. 1e), indicating that acetylation or lysine-to-arginine substitution at H3K56 does not substantially alter overall nucleosome spacing in chromatin templates, consistent with a previous report[13]. A bromodomain present in p300 can recognize an acetylated lysine, allowing p300 to acetylate other lysine residues on histone N-terminal tails, an effect that may further increase transcription[24]. However, our in vitro chromatin-acetylation assay showed that p53- and p300-dependent acetylation levels on four core histones of H3K56ac-chromatin were indistinguishable from those of unmodified-chromatin (Supplementary Fig. 1f). Furthermore, an in vitro transcription assay employing chromatin assembled with N-terminal tail-less histone octamers (Supplementary Fig. 1g), in which major histone acetylation sites in the N-terminal tails are removed[25], showed that H3K56ac still substantially increased transcription (~2.8-fold) (Fig. 1c, Supplementary Fig. 1h). These results indicate that the observed enhancement in transcription in the presence of H3K56ac is not mainly caused by p300-mediated acetylation at other lysine residues. The ATP-dependent chromatin remodeler ACF complex used in our recombinant chromatin assembly contains a bromodomain that can bind to acetylated histones[26]. An examination of transcription from chromatin templates assembled using the salt dialysis method[27] consistently demonstrated enhanced transcription (~3.0-fold) in H3K56ac-chromatin (Fig. 1d, Supplementary Fig. 1i), suggesting that H3K56ac-mediated transcriptional enhancement is not mainly attributable to inclusion of the ACF complex, at least in our transcription system.

Identification of the canonical BAF complex as an H3K56ac-nucleosome–interacting protein

On the basis of the above observations that H3K56ac does not substantially affect overall recombinant chromatin structure or stimulate acetylation on other lysine residues on histones, we speculated that the observed transcriptional enhancement with H3K56ac-chromatin is caused by effector(s) that recognizes H3K56ac. To search for nucleosomal H3K56ac-interacting proteins, we performed biotin pull-down using streptavidin-immobilized mononucleosomes as bait and nuclear extracts of HeLa S3 cells, and then identified proteins that differentially bound to H3K56ac-nucleosomes relative to unmodified nucleosomes by mass spectrometry (MS) (Fig. 2a).

We initially attempted these experiments using mononucleosomes assembled with a biotinylated 147-bp Widom 601 DNA sequence (N in Supplementary Fig. 2a, b), but failed to identify any proteins that specifically interacted with H3K56ac. Given the location of H3K56 at the DNA entry/exit point on the nucleosome[28], we repeated screens using mononucleosomes assembled with 217-bp DNA containing 35-bp extensions on both sides of the Widom 601 DNA sequence, which introduces some free DNA around H3K56 (35N35 in

https://doi.org/10.1038/s41467-024-53981-0

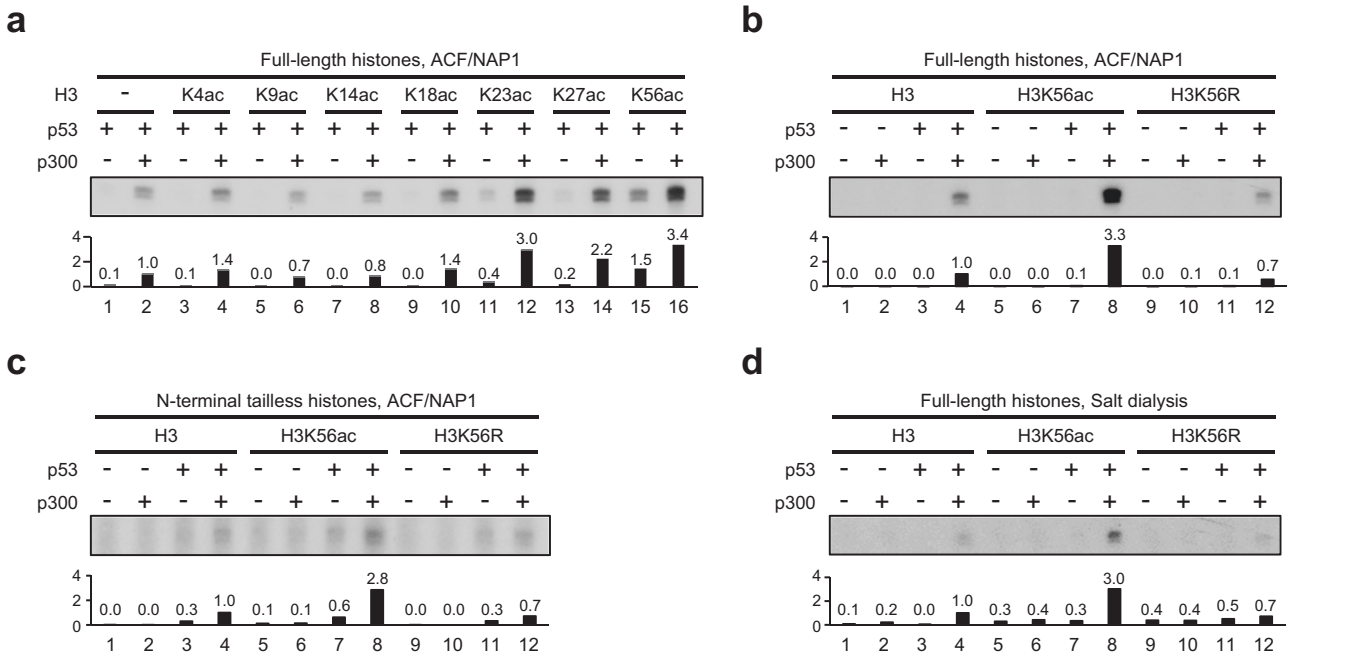

Fig. 1 | Enhanced transcription from H3K56ac-containing chromatin in vitro. p53- and p300-dependent transcription from recombinant chromatins containing full-length histone octamers harboring an individually acetylated lysine residue on H3 (**a**); full-length unmodified, H3K56ac and H3K56R histone octamers (**b**); and N-terminal tailless unmodified, H3K56ac, and H3K56R histone octamers (**c**), assembled using the ACF/NAP1 chromatin assembly system. **d** p53- and p300-dependent transcription from recombinant chromatins containing full-length unmodified, H3K56ac, and H3K56R histone octamers assembled using salt dialysis. Relative transcription levels were measured by autoradiography and normalized to those observed with the addition of p53 and p300 to chromatin containing unmodified histone octamers. Data are representative of at least two independent experiments. Source data are provided as a Source Data file.

Supplementary Fig. 2a, b). Among proteins identified in subsequent MS analysis, defined as those with 2-fold higher enrichment (p-value < 0.05) in H3K56ac-nucleosomes relative to unmodified nucleosomes, most were found to be subunits of the mSWI/SNF complex, a subfamily of ATP-dependent chromatin-remodeling complexes (Fig. 2b). The mSWI/SNF complex can be categorized into three distinct complexes – canonical BRG1/BRM-associated factor (BAF), polybromo-associated BAF (PBAF), and noncanonical BAF (ncBAF) – each of which contains common as well as complex-specific subunits[16] (Supplementary Fig. 2c). Interestingly, we found that all identified proteins were specific to the BAF complex or common to the mSWI/SNF complex (Fig. 2c). In support of our screens using streptavidin-coupled mononucleosomes and nuclear extracts, we found that H3K56ac-nucleosomes bound more strongly to the BAF-specific subunits, ARID1A and DPF2, than did unmodified nucleosomes (Fig. 2d). However, a PBAF-specific subunit (PHF10) showed no such preferred interaction with H3K56ac-nucleosomes, suggesting that nucleosomal H3K56ac preferentially interacts with the BAF complex among mSWI/SNF subfamily complexes. The weak interaction of subunits with unmodified nucleosomes may reflect the intrinsic ability of the mSWI/SNF complex to bind to the nucleosome as a chromatin remodeler[29,30].

The DPF domain in DPF2 is responsible for interaction of the BAF complex with H3K56ac-nucleosomes

To examine the direct interaction between the BAF complex and the H3K56ac-nucleosome, we prepared purified BAF complexes. Given that DPF2 is a BAF complex-specific subunit, we established a FLAG-DPF2 293 T cell line with a DPF2-knockout (KO) background (Supplementary Fig. 3a) and purified the complex by FLAG-affinity purification and subsequent glycerol gradient sedimentation (Supplementary Fig. 3b). Subsequent biotin pull-down (Fig. 3a) and gel shift (Fig. 3b) assays using purified BAF complex demonstrated preferential binding of the BAF complex to the H3K56ac-nucleosome. In a similar analysis, purified PBAF complex prepared from a FLAG-BRD7 293 T cell line with a BRD7-KO background (Supplementary Fig. 3c) showed that interactions with unmodified nucleosomes and H3K56ac-nucleosomes were indistinguishable (Supplementary Fig. 3d), confirming that, among mSWI/SNF subfamily complexes, the BAF complex specifically interacts with nucleosomal H3K56ac. Because paralogs exist for several subunits of the complex[15,31] (Supplementary Fig. 2c), the BAF complex purified from cell lines may contain heterogeneous components. To obtain a complex with a defined composition, we reconstituted and purified the BAF complex from Sf9 cells coinfected with baculoviruses that individually expressed FLAG-ARID1A and 10 untagged subunits (Supplementary Fig. 3e). Purified BAF complex containing defined subunits also showed increased interaction with H3K56ac-nucleosomes relative to unmodified nucleosomes (Supplementary Fig. 3f).

Next, we sought to identify the subunit within the BAF complex responsible for binding to H3K56ac. Several mSWI/SNF complex subunits contain domains that have the potential to interact with DNA or post-translationally modified histones[32] (Supplementary Fig. 2c). Among BAF complex subunits identified by our MS analysis, SMARCA4 and DPF2 were found to have a bromodomain and a double PHD finger (DPF) domain, respectively, capable of recognizing acetyl-lysine residues. Because the SMARCA4 subunit is common among mSWI/SNF complexes, we speculated that DPF2 is responsible for the direct interaction of the BAF complex with H3K56ac. In tests of this possibility, a biotin pull-down assay using nuclear extracts of DPF2-KO 293 T cells revealed that BAF complex subunits exhibited no difference in their interaction with unmodified nucleosomes compared with H3K56ac-nucleosomes (Supplementary Fig. 3g). Furthermore, DPF2-deficient BAF complex prepared by omitting DPF2 during baculovirus-mediated reconstitution (Supplementary Fig. 3h) showed that interactions with unmodified nucleosomes and H3K56ac-nucleosomes were indistinguishable (Supplementary Fig. 3i). We further found that purified DPF2 protein can selectively bind to H3K56ac-nucleosomes (Supplementary Fig. 3j, k). The weaker interaction of

https://doi.org/10.1038/s41467-024-53981-0

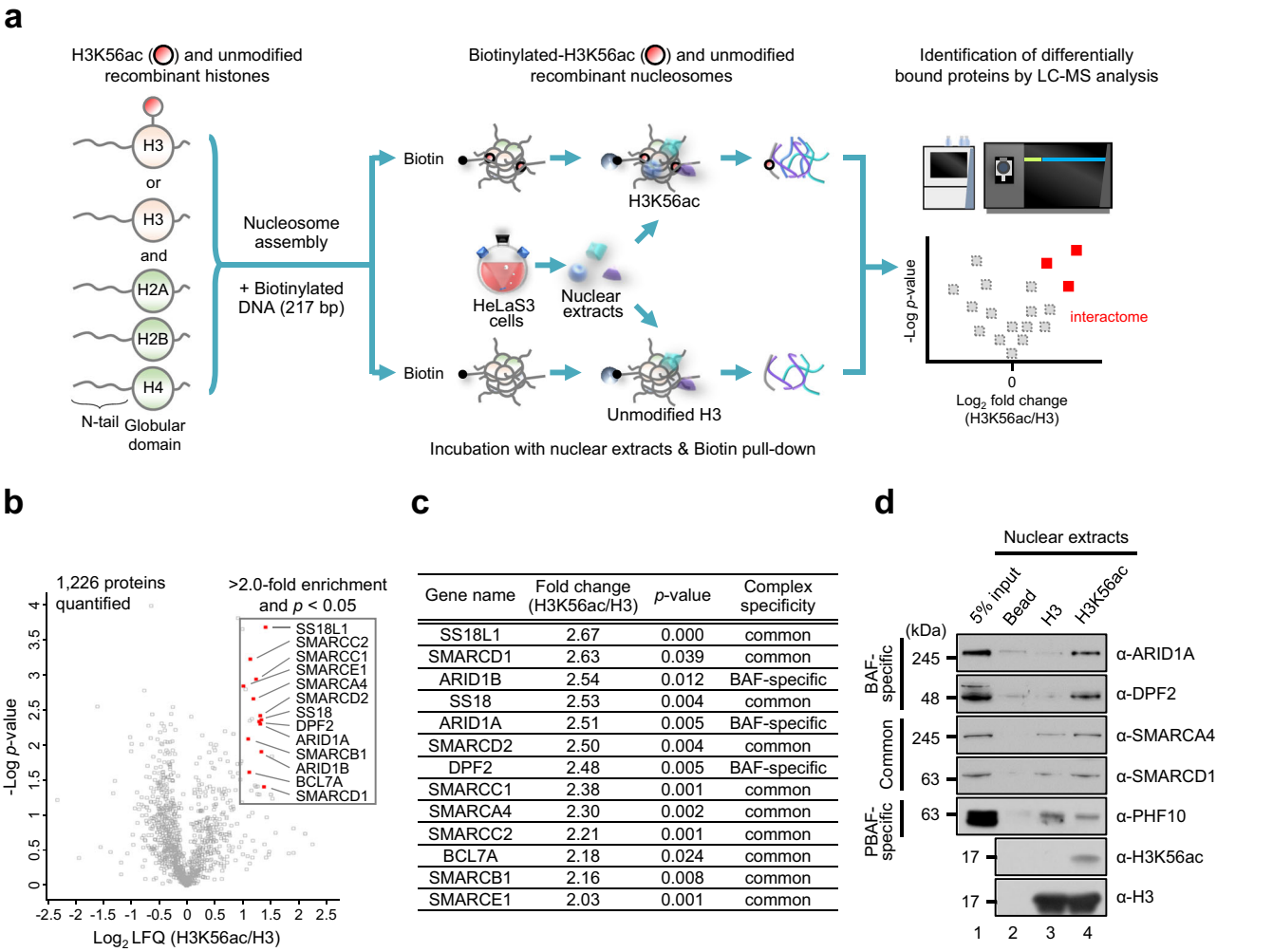

Gene name	Fold change (H3K56ac/H3)	*p*-value	Complex specificity
SS18L1	2.67	0.000	common
SMARCD1	2.63	0.039	common
ARID1B	2.54	0.012	BAF-specific
SS18	2.53	0.004	common
ARID1A	2.51	0.005	BAF-specific
SMARCD2	2.50	0.004	common
DPF2	2.48	0.005	BAF-specific
SMARCC1	2.38	0.001	common
SMARCA4	2.30	0.002	common
SMARCC2	2.21	0.001	common
BCL7A	2.18	0.024	common
SMARCB1	2.16	0.008	common
SMARCE1	2.03	0.001	common

Fig. 2 | Identification of nucleosomal H3K56ac-interacting proteins. **a** Schematic flow for identification of the H3K56ac-mononucleosome interactome. **b** Volcano plot for the nucleosomal H3K56ac interactome created using label-free quantitation (LFQ) intensity values and *p*-values measured from biotin pull-down and MS analysis. Two independent biological replicates were analyzed, and each biological replicate was measured in triplicate by liquid chromatography-mass spectrometry (LC-MS) analysis. Human canonical BAF complex subunits are depicted as red squares. **c** Summary of the BAF complex subunits enriched by biotin pull-down. *P*-values for the differences in protein abundance were determined by two-tailed unpaired Student's *t*-test (**b**, **c**). **d** Biotin pull-down assay using streptavidin-coupled mononucleosomes assembled with biotinylated 35N35 DNA and HeLa S3 nuclear extracts. Bound proteins were monitored by immunoblotting with the indicated antibodies. Data are representative of two independent experiments. Source data are provided as a Source Data file.

DPF2 alone compared with interaction of the BAF complex may indicate that DPF2 binding to H3K56ac-nucleosomes is more stable when DPF2 is part of the complex. The DPF domain in DPF2 was previously reported to recognize H3K14ac in an H3 N-terminal peptide[33] and regulate gene expression[34]. A comparison of binding efficiency showed that the BAF complex interacted comparably with H3K14ac- and H3K56ac-nucleosomes (Supplementary Fig. 1d, 2b, 3l), indicating that the BAF complex can recognize acetyl-lysine residues at different positions in the nucleosome with similar efficiency.

Coffin-Siris syndrome (CSS) (OMIM: 135900), a neurodevelopmental or cognitive disorder, is clinically diagnosed by the presence of heterozygous pathogenic variants in different BAF complex subunits, including DPF2[35,36]. Interestingly, we found that several CSS-associated mutations were concentrated in the DPF domain of DPF2[36] (Fig. 3c). To test the effect of CSS-associated mutations in DPF2 on binding of the BAF complex to H3K56ac-nucleosomes, we purified BAF complexes from a 293 T cell line that stably expresses FLAG-tagged CSS-associated DPF2 mutants (Supplementary Fig. 3m) and subjected them to nucleosome-binding assays. All tested DPF2 mutant-containing complexes exhibited reduced preferential interactions with H3K56ac-nucleosomes compared with the wild-type (WT) complex, reductions that were particularly notable for three such complexes (~5-fold), namely those harboring C330W, R350H, or W369R mutations (Fig. 3d). Collectively, these data demonstrate that the BAF complex recognizes nucleosomal H3K56ac through the DPF domain in DPF2.

H3K56ac enhances nucleosome remodeling and transcriptional activation by the BAF complex

Given that the BAF complex is an ATP-dependent chromatin remodeler, we tested whether H3K56ac can enhance the chromatin-remodeling activity of the BAF complex. To this end, we performed an in vitro restriction enzyme accessibility (REA) assay that employs purified BAF complex together with mononucleosomes assembled with 5′-rhodamine-labeled 347 bp DNA containing 100 bp extensions on both sides of a Widom 601 DNA sequence (100N100) (Supplementary Fig. 4a, b). In this assay, nucleosome remodeling can be measured by the appearance of ~174 bp DNA fragments produced by *Hha*I restriction enzyme digestion when the central position of the nucleosome is changed. Purified BAF complex exhibited nucleosome-remodeling activity on unmodified nucleosomes in an ATP- and incubation time-dependent manner (Fig. 4a). Importantly, we found that BAF complex-mediated nucleosome-remodeling activity was

https://doi.org/10.1038/s41467-024-53981-0

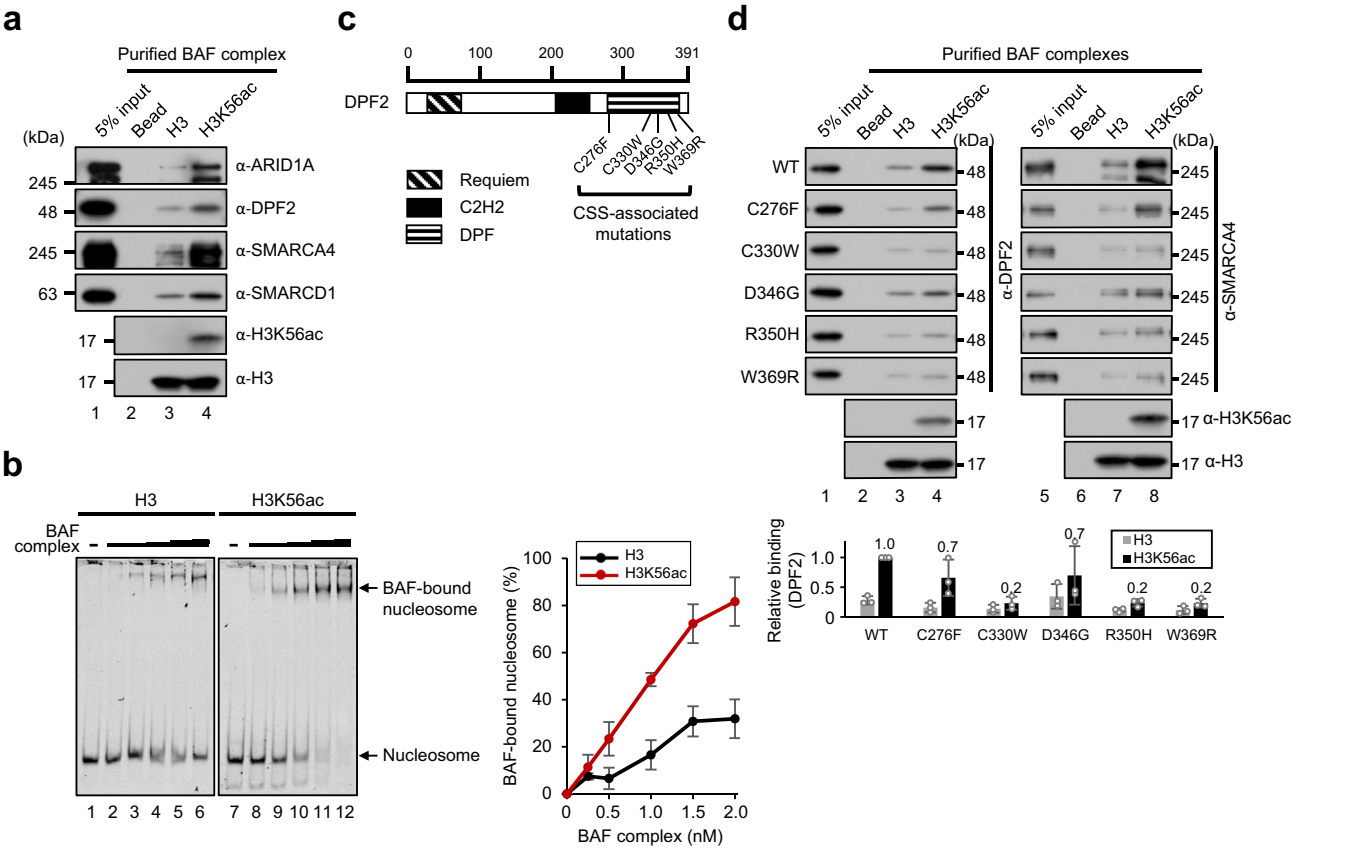

Fig. 3 | Direct interaction of the BAF complex with nucleosomal H3K56ac via the DPF2 subunit. a Biotin pull-down assay using streptavidin-coupled mononucleosomes and purified BAF complex. Data are representative of two independent experiments. **b** Gel shift assay using mononucleosomes assembled with rhodamine-labeled 35N35 DNA and different concentrations of purified BAF complex (0, 0.25, 0.5, 1.0, 1.5, and 2.0 nM). Left: Binding of the BAF complex to nucleosomes measured by fluorography. Right: Levels of BAF complex-bound nucleosomes were quantitated using ImageJ. Data are presented as mean values ± SD of three independent experiments. **c** Schematic diagram of human DPF2 with Requiem, C2H2 zinc finger, and DPF domains. Coffin-Siris syndrome (CSS)-associated missense mutations found in the DPF domain are indicated. Numbers indicate amino acid residues. **d** Biotin pull-down assay using streptavidin-coupled mononucleosomes and purified BAF complexes containing a mutation in the DPF domain of DPF2. Top: Binding of the BAF complexes to nucleosomes monitored by immunoblotting with anti-DPF2 and anti-SMARCA4 antibodies. Bottom: Protein levels of nucleosome-bound DPF2 of each complex were determined using ImageJ and normalized to those of DPF2 in input. The level of DPF2 binding to H3K56ac-nucleosomes in WT DPF2-containing complex was defined as 1. Data are presented as mean values ± SD of three independent experiments. Source data are provided as a Source Data file.

significantly increased on H3K56ac-nucleosomes relative to unmodified nucleosomes (up to 4.7-fold at 2 h). Furthermore, an in vitro nucleosome-sliding assay also revealed a largely enhanced nucleosome-remodeling activity of the BAF complex on H3K56ac-nucleosomes compared with unmodified nucleosomes (Supplementary Fig. 4c). To examine the relationship between H3K56ac interaction and nucleosome-remodeling activity, we performed REA assays using purified BAF complexes harboring CSS-associated DPF2 mutations (Supplementary Fig. 3m). All DPF2 mutant complexes showed diminished nucleosome-remodeling activity on H3K56ac-nucleosomes, with the R350H mutant showing the largest reduction (~ 3.4-fold at 2 h) and C276F and D346G mutants exhibiting lesser decreases, indicating a prominent role for DPF2 R350 in interactions with H3K56ac and the consequent enhanced nucleosome-remodeling activity of the BAF complex (Fig. 4b, Supplementary Fig. 4d).

The BAF complex was previously shown to interact with p53[37,38]. Thus, we tested the transcriptional coactivator function of the BAF complex in a p53-dependent in vitro chromatin-transcription assay in the presence and absence of H3K56ac, following the procedure outlined in Supplementary Fig. 4e. Reactions containing purified BAF complex stimulated transcription from unmodified chromatin up to 1.3-fold (Fig. 4c). Importantly, we observed that BAF complex-mediated transcriptional enhancement was further increased up to 2.0-fold in the presence of H3K56ac. Notably, this enhancement was diminished by up to 35% (~ 1.3-fold increase) in reactions containing the DPF2 R350H mutant BAF complex. These results suggest that the DPF2-mediated interaction with H3K56ac potentiates the chromatin-remodeling and transcriptional-coactivator functions of the BAF complex.

The DPF2 R350H mutation impairs p53-dependent gene expression

To investigate the effect of DPF2-mediated interactions of the BAF complex with H3K56ac on gene expression, we introduced the DPF2 R350H mutation into the genome of HCT116 cells using the CRISPR/Cas9 gene-editing system (Supplementary Fig. 5a). Homozygous and heterozygous DPF2 R350H mutant cells (H/H and R/H, respectively) were confirmed to express similar levels of DPF2 protein compared with WT cells (Supplementary Fig. 5b). Following on our examination of the function of H3K56ac–BAF complex interactions in p53-dependent transcription in vitro, we treated DPF2 WT and H/H cells with doxorubicin, a DNA-damaging agent, to induce p53 (Fig. 5a), and then carried out RNA sequencing analysis. We found that a total of 1352 genes were upregulated more than 1.5-fold upon doxorubicin treatment in WT cells (Fig. 5b) (1350 genes in H/H cells). We further found that doxorubicin-induced upregulation in a total of 202 genes was

https://doi.org/10.1038/s41467-024-53981-0

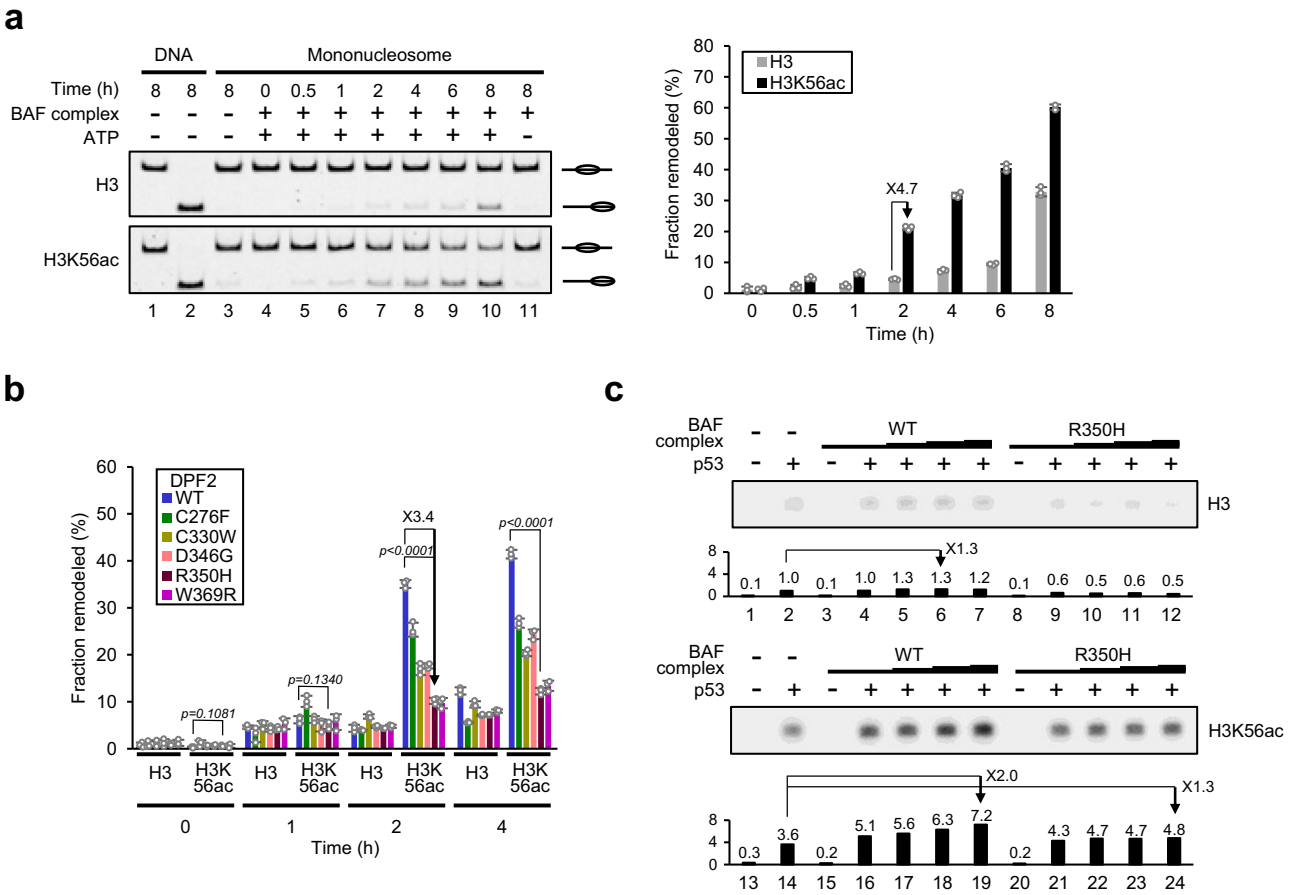

Fig. 4 | Enhanced nucleosome remodeling and transcriptional activity by the BAF complex in the presence of H3K56ac. a REA assay using mononucleosomes assembled with rhodamine-labeled 100N100 DNA and purified BAF complex. Left: Nucleosome-remodeling activity measured by fluorography. Note that the restriction enzyme, *Hha*I, was added to all reactions except lane 1. Right: Levels of remodeled nucleosomes were quantitated using ImageJ. Data are presented as mean values ± SD of three independent experiments. **b** REA assay with purified BAF complexes harboring a mutation in the DPF domain of DPF2. Data are presented as mean values ± SD of three independent experiments. *P*-values for the reactions with WT and R350H DPF2-containing complexes were determined by two-tailed unpaired Student's *t*-test. **c** In vitro chromatin-transcription assay with purified BAF complexes containing WT or R350H DPF2. Note that p300 was added to all reactions. Relative transcription levels were measured by autoradiography and normalized to those observed with the addition of p53 and p300 to chromatin containing unmodified histone octamers (lane 2). Data are representative of two independent experiments. Source data are provided as a Source Data file.

reduced to less than 0.5-fold in H/H cells compared with that in WT cells. Overlapping these two groups of genes found that, among the 1352 genes upregulated in WT, 75 showed decreased enhancement in expression in H/H cells (Fig. 5b, c). The substantial impairment in the transcriptional upregulation of these genes upon DNA damage is presumably attributable to the DPF2 R350H mutation. As expected, a KEGG (Kyoto Encyclopedia of Genes and Genomes) analysis revealed that these genes are primarily involved in the p53 signaling pathway and are associated with the cell cycle and apoptosis (Fig. 5d). In support of this, a quantitative reverse transcription-polymerase chain reaction (RT-qPCR) analysis found that upregulation of *p21*, *NOXA*, *KAI-I*, and *PAI-I* genes (representative of the 75 genes) upon doxorubicin treatment was substantially reduced in DPF2 mutant cells (Fig. 5e). The larger decreases in H/H than R/H cells indicates that a greater amount of BAF complex containing DPF2 R350H mutant results in more severe transcriptional defects in p53 signaling pathway genes.

Finally, we examined effects of the DPF2 R350H mutation on cellular DNA-damage responses. Doxorubicin-induced cytotoxicity caused a severe, concentration-dependent decrease in cell viability (Fig. 5f) and colony formation (Fig. 5g) in WT HCT116 cells. In p53-negative cells, used as a control, we found that the absence of p53 resulted in resistance to DNA damage owing to impaired cell cycle checkpoints[39]. Importantly, we found that DPF2 H/H mutant cells exhibited significantly reduced cytotoxicity relative to WT cells. We also found that apoptotic cell death induced by doxorubicin treatment was substantially impaired in DPF2 H/H mutant cells (Fig. 5h). Collectively, our results demonstrate that recognition of nucleosomal H3K56ac by DPF2 in the BAF complex and the resulting enhanced chromatin remodeling are important for p53-dependent gene expression and DNA-damage responses (Fig. 6).

Discussion

Conventional pull-down procedures using free histone peptides as bait have made major contributions to the identification of many important proteins that interact with post-translational modifications in histone N-terminal tails[7,40,41]. However, these approaches are inappropriate for histone globular domains, which lie within a well-organized structure, formed by intensive histone-histone and histone-DNA interactions, that provides a different environment for interacting proteins[9,10]. In supporting of this, and relevant to current study, we found that several bromodomain-containing proteins exhibited indistinguishable weak binding to both H3K56ac-nucleosomes and unmodified nucleosomes, despite the fact that these proteins were shown to preferentially bind to H3K56ac-peptide relative to unmodified-peptide[42]. In addition, previous studies reported that the PHD-Bromo tandem domain of tripartite motif-containing 66

https://doi.org/10.1038/s41467-024-53981-0

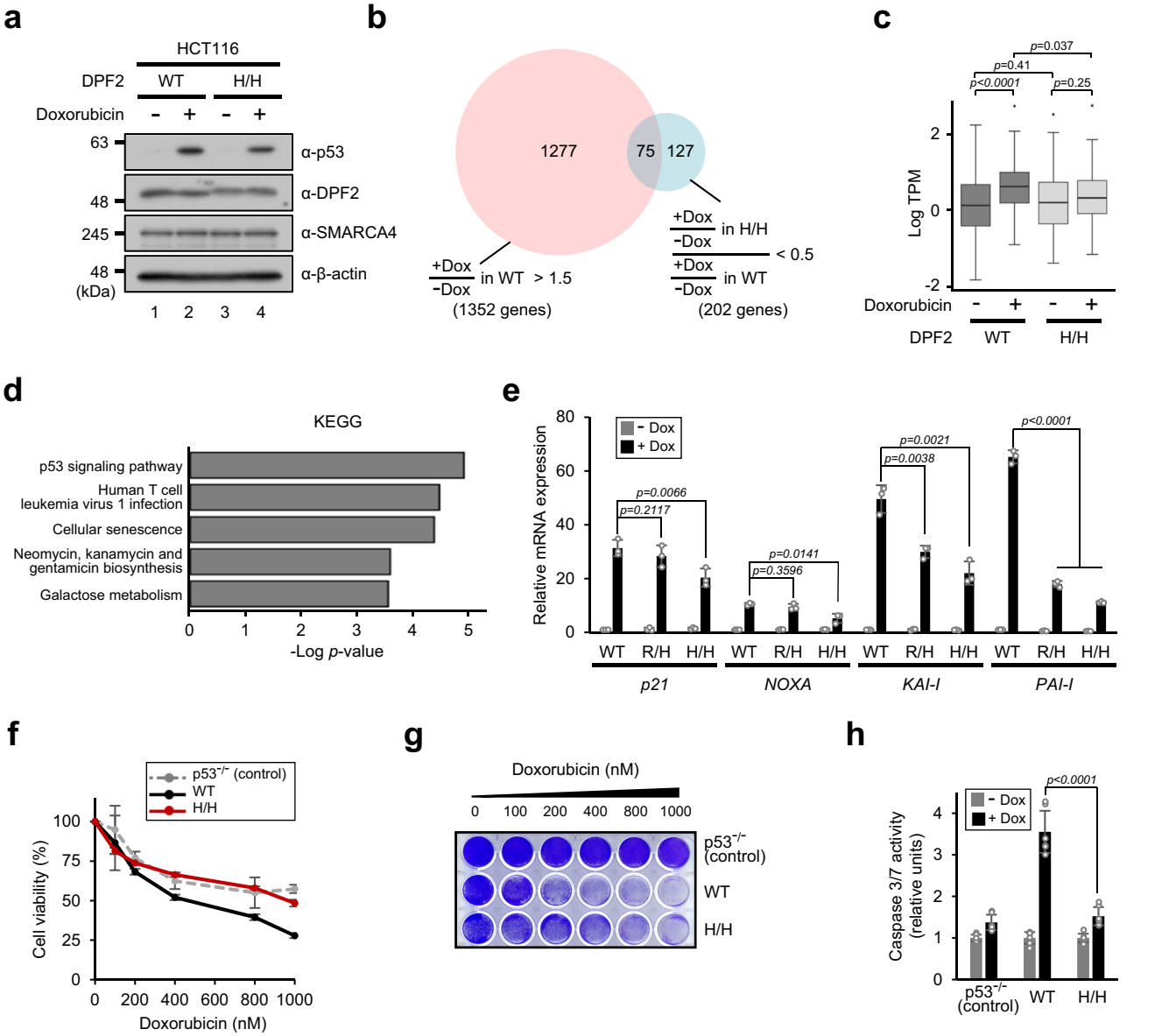

Fig. 5 | Impaired p53-dependent gene expression and DNA damage responses in DPF2 R350H mutant cells. a Doxorubicin-induced expression of p53. DPF2 WT and R350H (H/H) HCT116 cells were treated with 0.5 μM doxorubicin for 24 h, and protein levels were analyzed by immunoblotting. Data are representative of two independent experiments. **b** Venn diagram showing the overlap of genes upregulated (> 1.5-fold, FDR < 0.05) by doxorubicin treatment in WT cells and genes whose doxorubicin-induced upregulation in H/H cells was reduced to less than 0.5-fold compared with that in WT cells (FDR < 0.05). **c** Box plot displaying expression levels of the 75 overlapping genes in **b**. The box plots indicate the median (central line), the third and first quartiles (box edges), and 1.5 × interquartile range (IQR) above and below the box (whiskers) ($n = 1$ as biological replicates were combined). *P*-values were determined by two-tailed unpaired Student's *t*-test. TPM, transcripts per million. **d** KEGG (Kyoto Encyclopedia of Genes and Genomes) analysis of the 75 overlapping genes in **b**. The Fisher's exact test *p*-values were obtained using the GeneSCF functional enrichment tool. **e** mRNA levels of p53-dependent *p21*, *NOXA*, *KAI-I*, and *PAI-I* genes, with or without 0.5 μM doxorubicin treatment for 48 h, were measured by RT-qPCR and normalized to that of TBP mRNA. The levels of transcription of each gene in WT cells without doxorubicin treatment were defined as 1. Data are presented as mean values ± SD of three independent experiments. Cell-viability (**f**), colony-formation (**g**), and caspase-activity (**h**) assays using $p53^{-/-}$ (control) and DPF2 WT and H/H HCT116 cells. Cells were treated with different concentrations (0, 100, 200, 400, 800, and 1000 nM) (**f**, **g**) and 1000 nM (**h**) of doxorubicin. Data are presented as mean values ± SD of six independent experiments (**f**, **h**). Data are representative of three independent experiments (**g**). *P*-values were determined by two-tailed unpaired Student's *t*-test (**e**, **h**). Source data are provided as a Source Data file.

(TRIM66) and the bromodomain of CBP can recognize H3K56ac on peptides but not on nucleosomes[43,44]. Furthermore, in a direct comparison of peptides and nucleosomes, we found that the preferential interaction of the BAF complex with H3K56ac in a nucleosomal context did not occur in a parallel binding reaction with peptides composed of the 21 amino acids surrounding H3K56 (Supplementary Fig. 6). We also consistently observed decreased retention of SMARCA4 in the peptide-bound complex compared with other subunits, a phenomenon not evident in binding assays with nucleosomes. Collectively, these observations suggest that the use of physiologically irrelevant peptides can disrupt complex integrity, interfering with results of binding protein screens, and strongly suggest that the use of physiologically relevant nucleosomes as a bait is crucial to identifying globular domain-binding proteins.

Previous ChIP (chromatin immunoprecipitation) analyses have revealed preferential enrichment of H3K56ac around transcription start sites, transcription factor-binding sites, and promoter regions in various mammalian cell lines[45–47], implicating H3K56ac as an active

https://doi.org/10.1038/s41467-024-53981-0

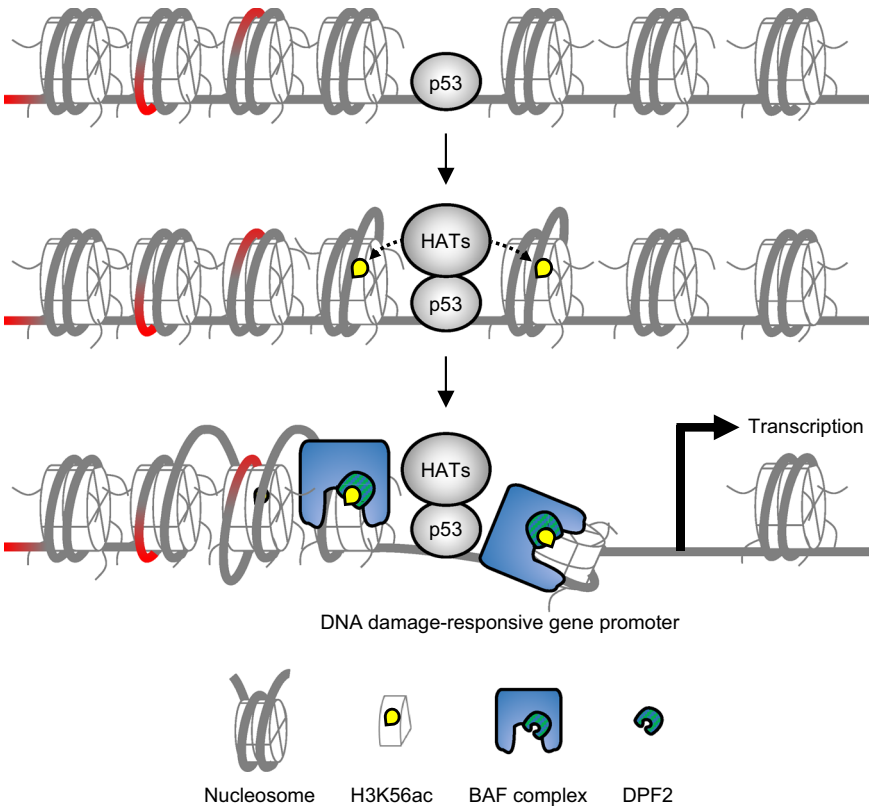

Fig. 6 | Schematic model of enhanced DNA damage-responsive gene expression mediated by H3K56ac-BAF complex interaction. Upon DNA damage (depicted by red-colored DNA), the tumor suppressor p53 is induced and binds to p53-responsive elements in the promoters of DNA damage-responsive genes. p53 recruits transcriptional coactivators, including histone acetyltransferases (HATs) such as p300 and CBP, to these promoter regions through direct interactions. HATs acetylate H3K56 located on the lateral surface of the histone globular domain. The chromatin remodeler BAF complex recognizes H3K56ac via the DPF domain in the DPF2 subunit and facilitates nucleosome remodeling around the promoter regions, thereby leading to enhanced gene expression. HATs also acetylate multiple lysine residues on histones and transcription factors (not depicted), further promoting efficient transcription.

transcription marker. The BAF complex is also considered to be involved in active transcription, as evidenced by the localization of several complex subunits at active gene promoters[48–50] and their direct interaction with the DNA-binding transcription activator, p53[37,38]. The direct interaction of the BAF complex with nucleosomal H3K56ac found in this study raises the question of whether the BAF complex and H3K56ac colocalize on actively transcribing genes, including DNA damage-responsive genes when cells experience DNA damage. However, in our search for suitable anti-H3K56ac antibodies for ChIP analysis, we found that all antibodies tested exhibited cross-reactivity toward H3 acetylated on other sites, especially H3K9ac (Supplementary Fig. 1a), consistent with previous reports of cross-reactivity of commercial anti-H3K56ac antibodies[51,52]. The similar amino acid sequences around H3K56 and other acetylation sites may account for the cross-reactivities of tested antibodies raised by peptide antigens. Considering the very low abundance of H3K56ac compared with other histone acetylations in human cells[51], it is reasonable to anticipate that the cross-reactivity of currently available anti-H3K56ac antibodies might result in misinterpretation when applied to ChIP analyses. The development of an antibody that specifically recognizes H3K56ac, ideally in a nucleosomal context, is crucial for accurately measuring colocalization of H3K56ac with interacting proteins.

A recent study elucidated the structure of the nucleosome-bound BAF complex[30]. According to this model, the nucleosome is sandwiched by the base and ATPase modules of the BAF complex. SMARCB1, within the head submodule in the base, directly binds to the histone octamer at the bottom of the nucleosome. Positioned just below SMARCB1 is the Requiem domain in the N-terminus of DPF2, comprising the head submodule and other subunits, bringing DPF2 into close proximity with the nucleosome. The absence of DPF2's C-terminal segment in the nucleosome-BAF structure suggest the flexible nature of this region, which encompasses the DPF domain. This proximity of DPF2 to the nucleosome could potentially allow the DPF domain to dock to H3K56 when it is acetylated, thereby strengthening the interaction of the BAF complex with the nucleosome. The DPF domain comprises PHD1 and PHD2 domains. An early nuclear magnetic resonance (NMR) spectroscopy study elucidating the binding of the DPF domain to the H3K14ac peptide revealed that PHD1 and PHD2 recognize H3K14ac and the N-terminal residues of H3, respectively[53]. Interestingly, our in vitro binding assays revealed that several purified BAF complexes containing CSS-associated mutations in the PHD2 domain exhibited impaired interaction with H3K56ac-nucleosomes but retained unaltered interaction with H3K14ac-nucleosomes (Supplementary Fig. 7). These results raise the possibility that the DPF domain in DPF2 may differentially recognize N-terminal tail- and globular domain-located histone acetylation. Further investigations, ideally involving structural analyses of the BAF complex in association with the H3K56ac-nucleosome, are warranted to comprehensively address these issues.

In addition to our research, a previous study revealed that the pluripotency transcription factor, Oct4, interacts with the H3K56ac-nucleosome[46]. These authors demonstrated that the presence of H3K56ac on nucleosomes facilitates the binding of Oct4 to adjacent DNA-binding sites in vitro, suggesting a role for H3K56ac in recruiting or stabilizing DNA-binding transcription factors at target genes. Another study highlighted the role of H3K122ac, located in the histone globular domain, in stimulating transcription[54]. Although the authors of this latter study did not identify specific H3K122ac-binding proteins,

they proposed that enhanced histone displacement in the presence of H3K122ac promotes the recruitment of transcription factors and RNA polymerase II to chromatin. Taken together with the results of our study, these findings indicate that acetylation on the histone globular domain participates in transcriptional regulation through multiple mechanisms, including direct effects on histone-DNA interaction and histone displacement as well as the recruitment of transcription factors.

In addition to H3K56ac, there are large numbers of globular domain modifications whose detailed molecular functions remain obscure. For instance, many lysine-acetylation, lysine-methylation, and serine-phosphorylation modifications in globular domains have been implicated in transcription, heterochromatin formation, and telomere silencing through their effects on DNA wrapping, nucleosome structure and nucleosome assembly, among other functions[10]. Importantly, there have been few reports on effector proteins that interact with most modifications in the globular domain. Moreover, the enzymes responsible for removal of these modifications and their physiological functions are largely unknown. Several methods employing genetic incorporation of modified amino acids in conjunction with subsequent chemical engineering techniques are currently available for the generation of histones that are homogeneously modified in the globular domain[13,55,56]. By virtue of its established experimental procedures for evaluating H3K56ac-interacting proteins, our study can be expanded to many globular domain modifications.

Methods

Recombinant histones and chromatin-assembly, and micrococcal nuclease-digestion assay

Recombinant *Xenopus laevis* core histones were purified and reconstituted into octamers as previously described[57]. Recombinant histone H3 harboring an acetylated lysine was prepared using the amber suppression method[58]. Briefly, pCDFDuet-1 plasmid (Millipore, 71340) containing H3 cDNA and AcKRS-pylT/pRSFDuet plasmid were co-transformed into *Escherichia coli* strain BL21 and H3 expression was induced with 1 mM Nε-Acetyl-L-lysine (Chem-Impex, 05364) and 0.5 mM IPTG (LabScientific, I-555). N-terminal His-tagged H3 was purified by IDA Excellose (Keyprogen, BPA003) chromatography, and the His-tag was removed by TEV protease cleavage. Recombinant chromatins for in vitro transcription assays were prepared using the ACF/NAP1 chromatin assembly system[59] or salt dialysis method[27]. For chromatin assembly using the ACF/NAP1 system, the reaction containing histone octamer and NAP1 in HEG buffer (25 mM HEPES [pH 7.5], 0.1 mM EDTA, and 10% glycerol) was incubated on ice for 30 min. The histone-NAP1 mix was further incubated with the ACF complex and plasmid in a reaction adjusted to 25 mM HEPES [pH 7.6], 50 mM KCl, 4.8 mM $MgCl_2$, 0.1 mM EDTA, 10% glycerol, and 3.4 mM ATP at 27 °C for 3 h. For chromatin assembly using the salt dialysis method, the reaction containing histone octamer and plasmid in TE buffer (10 mM Tris−Cl [pH 8.0] and 1 mM EDTA) supplemented with 1 M NaCl was incubated at 4 °C for 15 min. The histone-DNA mix was sequentially dialyzed against TE buffer containing 0.8, 0.6, and 0.05 M NaCl at room temperature for 2 h each. Recombinant mononucleosomes for biotin pull-down and nucleosome-remodeling assays were assembled using the salt dilution method[60]. Briefly, the reaction containing histone octamer and DNA in reaction buffer (10 mM Tris−Cl [pH 7.5], 2 M NaCl, 1 mM EDTA, and 10% glycerol) was incubated at 37 °C for 15 min. The histone-DNA mix was diluted by slowly adding buffer A (10 mM HEPES [pH 7.9], 1 mM EDTA, 5 mM DTT, and 0.5 mM PMSF) at 30 °C for 2 h, followed by the slow addition of buffer B (10 mM Tris−Cl [pH 7.5], 1 mM EDTA, 20% glycerol, 0.1% NP-40, 5 mM DTT, and 0.5 mM PMSF) at 30 °C for 30 min. For MNase digestion assays, recombinant chromatin was treated with 1 or 4 mU of MNase (Sigma, N5386) in reaction buffer (25 mM HEPES [pH 8.2], 50 mM KCl, 5 mM $MgCl_2$, 2 mM $CaCl_2$, 15% glycerol, and 3.2 mM ATP) containing 30 mM phosphocreatine (Sigma, P7936) and 3.6 μg ml^{-1} creatine phosphokinase (Sigma, C3755) at 25 °C for 10 min. Digested DNA was resolved on a 1.2% agarose gel and analyzed by ethidium bromide staining.

Immunoprecipitation of nucleosomal H3K56ac-interacting proteins

HeLa S3 nuclear extracts, prepared as described previously[61], were dialyzed against affinity purification (AP) buffer (50 mM HEPES [pH 7.5], 70 mM KOAc, and 5 mM $Mg(OAc)_2$) containing 0.2% (w/v) n-dodecyl-β-D-maltoside (DDM). Unmodified and H3K56ac-mononucleosomes were assembled with a 5′-biotinylated 217 bp DNA sequence containing 35-bp extensions on both sides of a 147 bp Widom 601 DNA sequence using the salt dilution method. Mononucleosomes (15 μg) immobilized on Pierce Streptavidin Plus UltraLink resin (Thermo Fisher Scientific, 53117) were incubated with nuclear extracts (1.2 mg) in AP buffer containing 150 mM KCl and 0.04% (w/v) DDM at 4 °C for 1 h, and bound proteins were eluted using MS buffer (100 mM Tris−Cl [pH 8.5]) containing 10 M urea. Eluates were adjusted to 8 M urea by adding MS buffer, reduced with Tris(2-carboxyethyl)-phosphine, and alkylated using 2-chloroacetamide. Proteins were then digested with 200 ng of Lys-C endoprotease (Wako, 121-05063) at 37 °C for 4 h. After the urea concentration was adjusted to 2 M with MS buffer, samples were further incubated with 200 ng of trypsin (Promega, V5280) at 37 °C for 16 h. Missed cleavage peptides were minimized by carrying out an additional digestion with 200 ng of trypsin at 37 °C for 4 h. Digested peptides were desalted on a reversed-phase C_{18} StageTips column[62], and the resulting eluants were dried in a vacuum concentrator and stored at −20 °C until subsequent analysis. Dried samples were resuspended in 0.1% formic acid prior to liquid chromatography-mass spectrometry (LC-MS) analysis.

Liquid chromatography-mass spectrometry

The LC-MS dataset was acquired using an EASY-nLC 1000 HPLC system coupled to an Orbitrap Eclipse Tribrid mass spectrometer (Thermo Fisher Scientific) equipped with a custom electrospray ionization source. Digested peptides were separated on a 150 mm reversed-phase analytical column (internal diameter, 75 μm) packed with C18 AQ resin (3 μm, 10 nm) (Bonna-Agela Technologies). Separation was performed using a 90 min, non-linear gradient of 5% − 95% acetonitrile at a flow rate of 350 nl min^{-1}. Full-scan survey mass spectra were collected (400 − 1,600 m/z) in Orbitrap utilizing an automatic gain control target of 400,000 ions with a resolution of 120,000. Tandem mass spectra were acquired using an automated gain control target of 50,000 ions with a resolution of 15,000. Charge states 2–7 precursor ions were selected for fragmentation. The most intense ions during a cycle time of 2 s were isolated and subjected to fragmentation using higher-energy collisional dissociation at 27% of the normalized energy. Two independent biological replicates were analyzed, and each biological replicate was measured in triplicate.

Mass spectrometry data analysis

MS peaks were generated from MS raw files using MaxQuant (version 1.6.8.0). The Andromeda peptide search engine in MaxQuant was used to match MS peaks against a concatenated UniProt human database (*Homo sapiens*, June 2020; 20,368 entries) and a decoy database constructed using modified reverse protein sequences, as described previously[63]. The search parameters were as follows: trypsin/P and LysC digestion, fixed carboxyamidomethyl modifications of cysteine, maximum of two missed cleavages, variable oxidation of methionine, variable acetylation of protein N-termini, variable acetylation of lysine, and variable carbamylation of peptide N-termini. Mass tolerances were 4.5 ppm and 20 ppm for precursor and fragment ions, respectively. Protein inference and quantitation were performed using MaxQuant with a 1% false discovery rate (FDR) threshold for both peptides and proteins. Abundances of identified proteins were inferred from

MaxLFQ intensities[64]. Statistical analyses and data representation were performed using Perseus (version 1.6.7.0)[65]. The statistical significance of differences in protein abundance was determined using a two-tailed Student's *t*-test.

Cell lines

293 T cells were purchased from ATCC (American Type Culture Collection, CRL-3216). HeLa S3, HCT116, and Sf9 cells were obtained from the Roeder lab at the Rockefeller University. For DPF2 and BRD7 knockouts (KO), two guide RNAs (gRNAs) per gene targeting different sites of the *DPF2* and *BRD7* genes were subcloned into pSpCas9(BB)−2A-GFP (Addgene, 48138) and pSpCas9(BB)−2A-RFP[66] plasmids. Plasmids were subsequently co-transfected into 293 T cells, and single cells positive for both GFP and RFP were isolated by fluorescence-activated cell sorting (FACS) (Supplementary Fig. 8a). KO was verified by immunoblot analysis and DNA sequencing of PCR products generated with primers bracketing gRNA target sites. gRNA sequences are summarized in Supplementary Information. For FLAG-DPF2 cell lines, pCAGIPuro plasmids expressing FLAG-tagged WT or mutant DPF2 were transfected into DPF2-KO 293 T cells, and single cells that stably expressed FLAG-DPF2 were selected by culturing in the presence of 2 μg ml^{-1} puromycin (Sigma, P8833). For DPF2 R350H cell lines, HCT116 cells were co-transfected with the pSpCas9(BB)−2A-GFP plasmid, expressing a gRNA targeting exon 10 of the *DPF2* gene, and a single-stranded oligodeoxynucleotide (ssODN) for introducing point mutation, and GFP-positive single cells were isolated by FACS (Supplementary Fig. 8b). Homozygous and heterozygous R350H mutant cells (H/H and R/H, respectively) were verified by genomic DNA sequencing of PCR products generated with primers bracketing gRNA target sites. gRNA and ssODN sequences are summarized in Supplementary Information.

Purification of the BAF complex

Affinity purification of the BAF complex from FLAG-DPF2 293 T cell lines was as described for purification of the human PAF1 complex[67]. Briefly, nuclear extracts derived from FLAG-DPF2 293 T cell lines were incubated with M2 agarose (Sigma, A2220) in BC buffer (20 mM Tris−Cl [pH 7.9], 0.2 mM EDTA, and 20% glycerol) containing 300 mM KCl (BC300; hereafter, the number indicates the KCl concentration added to the BC buffer) and 0.1% NP-40 at 4 °C for 4 h. After extensive washing with BC300 containing 0.1% NP-40, bound BAF complex was eluted with BC150 containing 0.3 mg ml^{-1} FLAG peptide and 0.1% NP-40. For baculovirus-mediated expression and purification of the BAF complex, cDNAs for human *ACTB* (Gene ID: 60), *ACTL6A* (86), *ARID1A* (8289), *BCL7A* (605), *DPF2* (5977), *SMARCA4* (6597), *SMARCB1* (6598), *SMARCC1* (6599), *SMARCD1* (6602), *SMARCE1* (6605), and *SS18L1* (26039) were PCR-amplified from the human cDNA library and subcloned into pFastBac1 plasmid (Thermo Fisher Scientific, 10360014), with or without an N-terminal FLAG-tag. Baculoviruses were generated according to the manufacturer's instructions (Thermo Fisher Scientific) and affinity purification was as described for purification of the human ZWC complex[68]. Briefly, Sf9 cells were infected with combinations of baculoviruses and incubated for 72 h. Cell extracts were prepared in BC300 containing 0.1% NP-40 supplemented with 1 mM DTT and 0.5 mM PMSF. Clarified extracts were incubated with M2 agarose at 4 °C for 4 h. After extensive washing with BC150 containing 0.1% NP-40, bound BAF complex was eluted with BC150 containing 0.25 mg ml^{-1} FLAG peptide and 0.1% NP-40. Affinity-purified BAF complexes from 293 T and Sf9 cells were further purified by density gradient centrifugation (10% − 30% glycerol gradient), and peak fractions were pooled.

In vitro transcription assay

In vitro transcription assays employing a chromatinized p53ML plasmid (containing five p53-binding sites and the adenovirus major late promoter, followed by a 390-nucleotide G-less cassette)[23] template were performed essentially as described previously[67]. Specifically, recombinant chromatin (containing 40 ng of DNA) was incubated with 10 ng of p53 in reaction buffer (10 mM HEPES [pH 7.8], 30 mM KCl, 2.5 mM DTT, 0.25 mM EDTA, and 5 mM sodium butyrate) at 30 °C for 20 min in a 20 μl reaction. p53-bound chromatin was incubated with the indicated amounts of purified BAF complex, 15 ng of p300, and 20 μM acetyl-CoA (Sigma, A2056) at 30 °C for 30 min in a 25 μl reaction. A preinitiation complex was formed by adding 5 μl of HeLa S3 cell-derived nuclear extracts (10 mg ml^{-1}) at 30 °C for 20 min. Transcription was performed at 30 °C for 40 min in a final volume of 50 μl containing 25 mM HEPES [pH 8.2], 60 mM KCl, 4 mM $MgCl_2$, 5 mM DTT, 15% glycerol, 0.5 mM ATP and CTP, 25 μM UTP, 0.1 mM 3′-O-methyl-GTP (APExBIO, B8038), 10 μCi [α-^{32}P] UTP (PerkinElmer, NEG507H), and 10 U RNasin (Promega, N2615). The reaction was stopped by adding 150 μl of stop buffer (150 mM sodium acetate [pH 5.2], 10 mM EDTA, and 0.5% SDS) and further incubated with 40 μg of proteinase K (Sigma, P6556) at 37 °C for 30 min. Radiolabeled RNA was extracted with phenol/chloroform/isoamyl alcohol (25:24:1), precipitated with ethanol, resolved on a 5% polyacrylamide gel (19:1) containing 8 M urea, and analyzed by autoradiography.

Nucleosome- and peptide-binding assays

For biotin pull-down assays, 25 pmol of mononucleosomes assembled with 5′-biotinylated 35N35 DNA or biotinylated peptides were immobilized on 15 μl of Pierce Streptavidin Plus UltraLink resin and incubated with 300 μg of nuclear extracts in AP buffer containing 150 mM KCl and 0.04% (w/v) DDM or 200 ng of purified proteins in binding buffer (20 mM Tris−Cl [pH 7.9], 150 mM KCl, 0.2 mM EDTA, 20% glycerol, and 0.05% NP-40) containing 0.2 mg ml^{-1} bovine serum albumen (BSA) at 4 °C for 1 h. The resin was then washed three times with AP buffer containing 150 mM KCl (for nuclear extracts) or binding buffer without BSA (for purified proteins), and bound proteins were monitored by immunoblot analysis. Peptide sequences used for binding assay are summarized in Supplementary Information. For gel shift assays, mononucleosomes (5 nM) assembled with rhodamine-labeled 35N35 DNA on both 5′-ends were incubated with the indicated amounts of purified BAF complex in 20 μl of binding buffer containing 1 mM DTT at 4 °C for 1 h. Nucleosomes were resolved by native polyacrylamide gel electrophoresis on 4% gels and visualized using a ChemiDoc MP imaging system (Bio-Rad).

Nucleosome-remodeling assay

For restriction enzyme accessibility (REA) assays, a mixture of purified BAF complex (0.5 nM) and mononucleosomes (5 nM) assembled with 100N100 DNA, labeled on both 5′-ends with rhodamine, was incubated at 30 °C for the indicated time in 20 μl of reaction buffer (25 mM Tris−OAc [pH 8.0], 150 mM KOAc, 1 mM $Mg(OAc)_2$, 1 mM DTT, 0.05 mg ml^{-1} BSA, and 3 mM ATP) containing 20 U *Hha*I. The reaction was stopped by adding 20 μl of quench buffer (20 mM Tris−OAc [pH 8.0], 80 mM EDTA, 1.2% SDS, and 20% sucrose) containing 30 U ml^{-1} proteinase K at 55 °C for 30 min. For nucleosome-sliding assays, mononucleosomes (5 nM) assembled with rhodamine-labeled 35N35 DNA on both 5′-ends were incubated with the indicated amounts of purified BAF complex in 20 μl of reaction buffer without BSA at 30 °C for 1 h. The reaction was halted by adding 400 ng of pGEM601 plasmid (Addgene, 221196). Samples were resolved by native polyacrylamide gel electrophoresis on 5% (REA assays) or 4% (nucleosome-sliding assays) gels and visualized using a ChemiDoc MP imaging system.

RNA sequencing analysis

Total RNA was prepared using TRIzol (Invitrogen, 15596026), and RNA libraries were generated using a TruSeq stranded mRNA library kit (Illumina). RNA sequencing was performed on a NovaSeq 6000 sequencer (Illumina) using the paired-end method (100 bp

reads). Reads were aligned to the hg38 human reference genome using STAR v2.7.5a[69], and the number of mapped reads was counted using featureCounts v1.5.0-p1[70]. Differentially expressed genes were analyzed using DESeq2 v1.36.0[71]. Transcripts per million (TPM) counts for boxplots were obtained using TPMCalculator v0.0.3[72]. KEGG analyses were performed using GeneSCF v1.1[73].

Quantitative RT-PCR analysis

Total RNA was prepared using TRIzol, cDNA was synthesized by reverse transcription using PrimeScript RT Master Mix (Takara, RR036A), and qPCR was performed using TOPreal SYBR Green qPCR PreMIX (Enzynomics, RT500). Data were analyzed by calculating ΔCq, normalized to TATA-binding protein (TBP) mRNA expression. Primers for qPCR reactions are summarized in Supplementary Information.

Cell-viability, colony-formation, and caspase-activity assays

For cell-viability assays, HCT116 cells were treated with the indicated concentration of doxorubicin for 48 h, and luminescence signals – proportional to the amount of ATP in viable cells – were measured using a CellTiter-Glo Luminescent Cell Viability Assay kit (Promega, G7571). For colony-formation assays, cells were treated with the indicated concentration of doxorubicin for 6 days, stained with crystal violet solution (137 mM NaCl, 2.7 mM KCl, 10 mM Na_2HPO_4, 1.8 mM KH_2PO_4, 1% formaldehyde, 1% methanol, and 0.05% crystal violet (Sigma, V5265)) for 20 min, washed with water, and air-dried. For the caspase-activity assay, cells were left untreated or were treated with 1 μM doxorubicin for 48 h, and caspase-3 and −7 activities were measured using a Caspase-Glo 3/7 Assay kit (Promega, G8091) and a CentroPRO LB 962 microplate luminometer (Berthold Technologies).

Antibodies

The following antibodies were obtained commercially: anti-ACTB (OriGene, TA811000); anti-ACTL6A (Santa Cruz Biotechnology, sc-137062); anti-ARID1A (Cell Signaling Technology, 12354S); anti-BCL7A (Atlas Antibodies, HPA019762); anti-DPF2 (Abcam, ab128149); anti-PHF10 (Abcam, ab154637); anti-p53 (Abcam, ab1101); anti-SMARCA4 (Cell Signaling Technology, 49360S); anti-SMARCB1 (Santa Cruz Biotechnology, sc-166165); anti-SMARCC1 (Santa Cruz Biotechnology, sc-32763); anti-SMARCD1 (Santa Cruz Biotechnology, sc-135843); anti-SMARCE1 (Abcam, ab137081); anti-SS18L1 (Abcam, ab227535); anti-H2B (Abcam, ab1790); anti-H3 (Millipore, 05-928); anti-H3K4ac (Active Motif, 39381); anti-H3K9ac (Cell Signaling Technology, 9649S); anti-H3K14ac (Abcam, ab52946); anti-H3K18ac (Millipore, 07-354); anti-H3K23ac (Millipore, 07-355); anti-H3K27ac (Millipore, 07-360); anti-H3K56ac (Abcam, ab76307; Active Motif, 39281 and 91127; Cell Signaling Technology, 4243S; Sigma, SAB5600015); and anti-FLAG (Sigma, F3165). Note that the anti-H3K56ac antibody from Sigma was used for all anti-H3K56ac immunoblot analyses, except for Supplementary Fig. 1a, which includes a comparative analysis of multiple anti-H3K56ac antibodies.

Statistics and reproducibility

The sample size was determined based on our experience and reports from previously published studies with similar experiments. Two-tailed Student's *t*-tests were used to analyze data from mass spectrometry, nucleosome remodeling, gene expression, apoptosis, and protein expression experiments. The GeneSCF functional enrichment tool was used to calculate Fisher's exact test *p*-values for KEGG analysis. All statistical methods are detailed in the figure legends. Data are presented as mean values ± standard deviation (SD), with *p*-values below 0.05 considered statistically significant.

Reporting summary

Further information on research design is available in the Nature Portfolio Reporting Summary linked to this article.

Data availability

Mass spectrometry data generated in this study have been deposited in the ProteomeXchange Consortium via the jPOST partner repository with the dataset identifier ProteomeXchange: PXD051883 and jPOST: JPST003064. RNA-seq data generated in this study have been deposited in the Gene Expression Omnibus under accession number GSE266321. Source data are provided with this paper.

References

1. Patel, D. J. & Wang, Z. Readout of epigenetic modifications. *Annu. Rev. Biochem.* **82**, 81–118 (2013).
2. Millán-Zambrano, G., Burton, A., Bannister, A. J. & Schneider, R. Histone post-translational modifications - cause and consequence of genome function. *Nat. Rev. Genet.* **23**, 563–580 (2022).
3. Mohammad, H. P., Barbash, O. & Creasy, C. L. Targeting epigenetic modifications in cancer therapy: erasing the roadmap to cancer. *Nat. Med.* **25**, 403–418 (2019).
4. Zhao, S., Allis, C. D. & Wang, G. G. The language of chromatin modification in human cancers. *Nat. Rev. Cancer* **21**, 413–430 (2021).
5. Janssen, S. M. & Lorincz, M. C. Interplay between chromatin marks in development and disease. *Nat. Rev. Genet.* **23**, 137–153 (2022).
6. Rothbart, S. B. & Strahl, B. D. Interpreting the language of histone and DNA modifications. *Biochim. Biophys. Acta Gene Regul. Mech.* **1839**, 627–643 (2014).
7. Wilkinson, A. W. & Gozani, O. Histone-binding domains: strategies for discovery and characterization. *Biochim. Biophys. Acta Gene Regul. Mech.* **1839**, 669–675 (2014).
8. Kebede, A. F., Schneider, R. & Daujat, S. Novel types and sites of histone modifications emerge as players in the transcriptional regulation contest. *FEBS J.* **282**, 1658–1674 (2015).
9. Tessarz, P. & Kouzarides, T. Histone core modifications regulating nucleosome structure and dynamics. *Nat. Rev. Mol. Cell Biol.* **15**, 703–708 (2014).
10. Lawrence, M., Daujat, S. & Schneider, R. Lateral thinking: how histone modifications regulate gene expression. *Trends Genet* **32**, 42–56 (2016).
11. Xu, F., Zhang, K. & Grunstein, M. Acetylation in histone H3 globular domain regulates gene expression in yeast. *Cell* **121**, 375–385 (2005).
12. Li, Q. et al. Acetylation of histone H3 lysine 56 regulates replication-coupled nucleosome assembly. *Cell* **134**, 244–255 (2008).
13. Neumann, H. et al. A method for genetically installing site-specific acetylation in recombinant histones defines the effects of H3 K56 acetylation. *Mol. Cell* **36**, 153–163 (2009).
14. Vignali, M., Hassan, A. H., Neely, K. E. & Workman, J. L. ATP-dependent chromatin-remodeling complexes. *Mol. Cell. Biol.* **20**, 1899–1910 (2000).
15. Kadoch, C. et al. Proteomic and bioinformatic analysis of mammalian SWI/SNF complexes identifies extensive roles in human malignancy. *Nat. Genet.* **45**, 592–601 (2013).
16. Centore, R. C., Sandoval, G. J., Soares, L. M. M., Kadoch, C. & Chan, H. M. Mammalian SWI/SNF chromatin remodeling complexes: emerging mechanisms and therapeutic strategies. *Trends Genet* **36**, 936–950 (2020).
17. Shain, A. H. & Pollack, J. R. The spectrum of SWI/SNF mutations, ubiquitous in human cancers. *PLoS ONE* **8**, e55119 (2013).
18. Pulice, J. L. & Kadoch, C. Composition and function of mammalian SWI/SNF chromatin remodeling complexes in human disease. *Cold Spring Harb. Symp. Quant. Biol.* **81**, 53–60 (2016).
19. Reddy, D., Bhattacharya, S. & Workman, J. L. (mis)-Targeting of SWI/SNF complex(es) in cancer. *Cancer Metastasis Rev.* **42**, 455–470 (2023).
20. Kouzarides, T. Chromatin modifications and their function. *Cell* **128**, 693–705 (2007).

21. Li, B., Carey, M. & Workman, J. L. The role of chromatin during transcription. *Cell* **128**, 707–719 (2007).
22. Shvedunova, M. & Akhtar, A. Modulation of cellular processes by histone and non-histone protein acetylation. *Nat. Rev. Mol. Cell Biol.* **23**, 329–349 (2022).
23. An, W., Kim, J. & Roeder, R. G. Ordered cooperative functions of PRMT1, p300, and CARM1 in transcriptional activation by p53. *Cell* **117**, 735–748 (2004).
24. Kikuchi, M. et al. Epigenetic mechanisms to propagate histone acetylation by p300/CBP. *Nat. Commun.* **14**, 4103 (2023).
25. An, W., Palhan, V. B., Karymov, M. A., Leuba, S. H. & Roeder, R. G. Selective requirements for histone H3 and H4 N termini in p300-dependent transcriptional activation from chromatin. *Mol. Cell* **9**, 811–821 (2002).
26. Nightingale, K. P. et al. Acetylation increases access of remodelling complexes to their nucleosome targets to enhance initiation of V(D) J recombination. *Nucleic Acids Res.* **35**, 6311–6321 (2007).
27. Cruz-Becerra, G. & Kadonaga, J. T. Reconstitution of chromatin by stepwise salt dialysis. *Bio Protoc.* **11**, e3977 (2021).
28. Davey, C. A., Sargent, D. F., Luger, K., Maeder, A. W. & Richmond, T. J. Solvent mediated interactions in the structure of the nucleosome core particle at 1.9 a resolution. *J. Mol. Biol.* **319**, 1097–1113 (2002).
29. Han, Y., Reyes, A. A., Malik, S. & He, Y. Cryo-EM structure of SWI/SNF complex bound to a nucleosome. *Nature* **579**, 452–455 (2020).
30. He, S. et al. Structure of nucleosome-bound human BAF complex. *Science* **367**, 875–881 (2020).
31. Mashtalir, N. et al. Modular organization and assembly of SWI/SNF family chromatin remodeling complexes. *Cell* **175**, 1272–1288 (2018).
32. Wanior, M., Krämer, A., Knapp, S. & Joerger, A. C. Exploiting vulnerabilities of SWI/SNF chromatin remodelling complexes for cancer therapy. *Oncogene* **40**, 3637–3654 (2021).
33. Huber, F. M. et al. Histone-binding of DPF2 mediates its repressive role in myeloid differentiation. *Proc. Natl. Acad. Sci. USA* **114**, 6016–6021 (2017).
34. Soshnikova, N. V., Sheynov, A. A., Tatarskiy, E. V. & Georgieva, S. G. The DPF domain as a unique structural unit participating in transcriptional activation, cell differentiation, and malignant transformation. *Acta Nat.* **12**, 57–65 (2020).
35. Kosho, T. & Okamoto, N. Genotype-phenotype correlation of Coffin-Siris syndrome caused by mutations in SMARCB1, SMARCA4, SMARCE1, and ARID1A. *Am. J. Med. Genet. C. Semin. Med. Genet.* **166c**, 262–275 (2014).
36. Vasileiou, G. et al. Mutations in the BAF-complex subunit DPF2 are associated with coffin-siris syndrome. *Am. J. Hum. Genet.* **102**, 468–479 (2018).
37. Lee, D. et al. SWI/SNF complex interacts with tumor suppressor p53 and is necessary for the activation of p53-mediated transcription. *J. Biol. Chem.* **277**, 22330–22337 (2002).
38. Oh, J. et al. BAF60a interacts with p53 to recruit the SWI/SNF complex. *J. Biol. Chem.* **283**, 11924–11934 (2008).
39. Vousden, K. H. & Prives, C. Blinded by the light: the growing complexity of p53. *Cell* **137**, 413–431 (2009).
40. Wysocka, J. Identifying novel proteins recognizing histone modifications using peptide pull-down assay. *Methods* **40**, 339–343 (2006).
41. Voigt, P. & Reinberg, D. Histone tails: ideal motifs for probing epigenetics through chemical biology approaches. *ChemBioChem* **12**, 236–252 (2011).
42. Filippakopoulos, P. et al. Histone recognition and large-scale structural analysis of the human bromodomain family. *Cell* **149**, 214–231 (2012).
43. Xu, L. et al. Structural insight into the recognition of acetylated histone H3K56ac mediated by the bromodomain of CREB-binding protein. *FEBS J.* **284**, 3422–3436 (2017).
44. Chen, J. et al. TRIM66 reads unmodified H3R2K4 and H3K56ac to respond to DNA damage in embryonic stem cells. *Nat. Commun.* **10**, 4273 (2019).
45. Lo, K. A. et al. Genome-wide profiling of H3K56 acetylation and transcription factor binding sites in human adipocytes. *PLoS ONE* **6**, e19778 (2011).
46. Tan, Y., Xue, Y., Song, C. & Grunstein, M. Acetylated histone H3K56 interacts with Oct4 to promote mouse embryonic stem cell pluripotency. *Proc. Natl. Acad. Sci. USA* **110**, 11493–11498 (2013).
47. Jain, A. K. et al. LncPRESS1 is a p53-regulated lncRNA that safeguards pluripotency by disrupting SIRT6-mediated de-acetylation of histone H3K56. *Mol. Cell* **64**, 967–981 (2016).
48. Brahma, S. & Henikoff, S. The BAF chromatin remodeler synergizes with RNA polymerase II and transcription factors to evict nucleosomes. *Nat. Genet.* **56**, 100–111 (2024).
49. Martin, B. J. E. et al. Global identification of SWI/SNF targets reveals compensation by EP400. *Cell* **186**, 5290–5307 (2023).
50. Golov, A. K., Gavrilov, A. A., Kaplan, N. & Razin, S. V. A genome-wide nucleosome-resolution map of promoter-centered interactions in human cells corroborates the enhancer-promoter looping model. Preprint at https://doi.org/10.7554/eLife.91596.1 (2023).
51. Drogaris, P. et al. Histone deacetylase inhibitors globally enhance h3/h4 tail acetylation without affecting h3 lysine 56 acetylation. *Sci. Rep.* **2**, 220 (2012).
52. Pal, S. et al. The commercial antibodies widely used to measure H3 K56 acetylation are non-specific in human and drosophila cells. *PLoS ONE* **11**, e0155409 (2016).
53. Zeng, L. et al. Mechanism and regulation of acetylated histone binding by the tandem PHD finger of DPF3b. *Nature* **466**, 258–262 (2010).
54. Tropberger, P. et al. Regulation of transcription through acetylation of H3K122 on the lateral surface of the histone octamer. *Cell* **152**, 859–872 (2013).
55. Lee, S. et al. A facile strategy for selective incorporation of phosphoserine into histones. *Angew. Chem. Int. Ed. Engl.* **52**, 5771–5775 (2013).
56. Yang, A. et al. A chemical biology route to site-specific authentic protein modifications. *Science* **354**, 623–626 (2016).
57. Luger, K., Rechsteiner, T. J., Flaus, A. J., Waye, M. M. & Richmond, T. J. Characterization of nucleosome core particles containing histone proteins made in bacteria. *J. Mol. Biol.* **272**, 301–311 (1997).
58. Umehara, T. et al. N-acetyl lysyl-tRNA synthetases evolved by a CcdB-based selection possess N-acetyl lysine specificity in vitro and in vivo. *FEBS Lett.* **586**, 729–733 (2012).
59. Ito, T. et al. ACF consists of two subunits, Acf1 and ISWI, that function cooperatively in the ATP-dependent catalysis of chromatin assembly. *Genes Dev.* **13**, 1529–1539 (1999).
60. Steger, D. J., Eberharter, A., John, S., Grant, P. A. & Workman, J. L. Purified histone acetyltransferase complexes stimulate HIV-1 transcription from preassembled nucleosomal arrays. *Proc. Natl. Acad. Sci. USA* **95**, 12924–12929 (1998).
61. Dignam, J. D., Lebovitz, R. M. & Roeder, R. G. Accurate transcription initiation by RNA polymerase II in a soluble extract from isolated mammalian nuclei. *Nucleic Acids Res.* **11**, 1475–1489 (1983).
62. Rappsilber, J., Mann, M. & Ishihama, Y. Protocol for micro-purification, enrichment, pre-fractionation and storage of peptides for proteomics using StageTips. *Nat. Protoc.* **2**, 1896–1906 (2007).
63. Cox, J. & Mann, M. MaxQuant enables high peptide identification rates, individualized p.p.b.-range mass accuracies and proteome-wide protein quantification. *Nat. Biotechnol.* **26**, 1367–1372 (2008).
64. Cox, J. et al. Accurate proteome-wide label-free quantification by delayed normalization and maximal peptide ratio extraction, termed MaxLFQ. *Mol. Cell. Proteom.* **13**, 2513–2526 (2014).

65. Tyanova, S., Temu, T. & Cox, J. The MaxQuant computational platform for mass spectrometry-based shotgun proteomics. *Nat. Protoc.* **11**, 2301–2319 (2016).
66. Bunina, D. et al. Genomic rewiring of SOX2 chromatin interaction network during differentiation of ESCs to postmitotic neurons. *Cell Syst.* **10**, 480–494 (2020).
67. Kim, J., Guermah, M. & Roeder, R. G. The human PAF1 complex acts in chromatin transcription elongation both independently and cooperatively with SII/TFIIS. *Cell* **140**, 491–503 (2010).
68. Park, K. et al. ZWC complex-mediated SPT5 phosphorylation suppresses divergent antisense RNA transcription at active gene promoters. *Nucleic Acids Res.* **50**, 3835–3851 (2022).
69. Dobin, A. et al. STAR: ultrafast universal RNA-seq aligner. *Bioinformatics* **29**, 15–21 (2013).
70. Liao, Y., Smyth, G. K. & Shi, W. featureCounts: an efficient general purpose program for assigning sequence reads to genomic features. *Bioinformatics* **30**, 923–930 (2014).
71. Love, M. I., Huber, W. & Anders, S. Moderated estimation of fold change and dispersion for RNA-seq data with DESeq2. *Genome Biol.* **15**, 550 (2014).
72. Vera Alvarez, R., Pongor, L. S., Mariño-Ramírez, L. & Landsman, D. TPMCalculator: one-step software to quantify mRNA abundance of genomic features. *Bioinformatics* **35**, 1960–1962 (2019).
73. Subhash, S. & Kanduri, C. GeneSCF: a real-time based functional enrichment tool with support for multiple organisms. *BMC Bioinform.* **17**, 365 (2016).

Acknowledgements

This work was supported by the Samsung Science and Technology Foundation (SSTF-BA1702-13 to J.K.) and National Research Foundation of Korea (NRF-2022R1A2C3012803 and NRF-2018R1A5A1024261 to J.K. and NRF-2021R1A6A3A01087387 to K.H.).

Author contributions

K.H. and Jaehoon K. designed the research and wrote the manuscript with assistance from all authors. K.H. performed all biochemical and cellular studies with support from J.A. and H.K. Jihyun K., Y.I.K. and J.E.L. performed immunoprecipitation-mass spectrometry experiments and analyzed the data. H.S.P. and R.G.R. provided experimental advice and discussion.

Competing interests

The authors declare no competing interests.

Additional information

Supplementary information The online version contains supplementary material available at https://doi.org/10.1038/s41467-024-53981-0.

Correspondence and requests for materials should be addressed to J. Eugene Lee or Jaehoon Kim.

Peer review information *Nature Communications* thanks Lu Wang, Jerry Workman and the other, anonymous, reviewer(s) for their contribution to the peer review of this work. A peer review file is available.